Journal of Alloys and Compounds 516 (2012) 179–185

Contents lists available at SciVerse ScienceDirect

Journal of Alloys and Compounds

journal homepage: www.elsevier.com/locate/jallcom

Synthesis process and structural characterization of the Sr_2EuRuO_6 complex perovskite

C.A. Triana, D.A. Landínez Téllez, J. Roa-Rojas*

Grupo de Física de Nuevos Materiales (GFNM), Departamento de Física, Universidad Nacional de Colombia, Bogotá D.C. A.A. 5997, Colombia

ARTICLE INFO

Article history:
Received 6 September 2011
Received in revised form 2 December 2011
Accepted 11 December 2011
Available online 20 December 2011

Keywords:
X-ray powder diffraction
Complex perovskite
Crystal structure
Electron microscopy
Energy dispersive X-ray

ABSTRACT

The Sr_2EuRuO_6 complex perovskite has been synthesized by the solid-state reaction method and the crystal structure, surface morphology and composition have been investigated. Results of powder X-ray diffraction measurements and Rietveld analysis show that this compound crystallizes in a monoclinic distorted perovskite-type structure, which belongs to the monoclinic $P2_1/n$ (#14) space group, that corresponds to the $(a^+b^-b^-)$ tilt system on the Glazer notation. The structure presents an alternating distribution of the Ru^{5+} and Eu^{3+} ions on the six coordinate M sites, while the Sr^{2+} is located in the A-site of the Sr_2EuRuO_6 complex perovskite, with lattice parameters $a = 5.7996(5)$ Å, $b = 5.8960(7)$ Å, $c = 8.3234(6)$ Å, angle $\beta = 90.234(7)^\circ$ and $V = 284.61(4)$ Å^3. Morphological analysis of this material, performed by scanning electron microscopy (SEM), allows to establish the granular feature of compound with agglomerates from amongst ≈1 to 3 μm size, and by means of the Scherrer formula was calculated a particle size of $D = 34.2$ nm. Result suggests that crystal structure of the Sr_2EuRuO_6 suffers grain size-induced polarization rotation, which produces a phase transition toward monoclinic phase $P2_1/n$ (#14). The activation energy E_a is close to $E_a = 39.6$ kJ/mol. Suggesting that during the sintering process of the Sr_2EuRuO_6 is delivering oxygen species that should in fact lower the activation energy E_a of the compound. Semi-quantitative compositional study was carried out from energy dispersive X-ray (EDX) experiments in order to obtain the independent elements percentage of the Sr_2EuRuO_6 complex perovskite.

1. Introduction

The complex perovskite-type oxides have the general formula $A_2M'M''O_6$, in which the cation A is an alkaline earth metal, M′ corresponds to *3d* transition metal and M″ is a transition metal. M′ and M″ have different oxidation states and these cations define the physical properties of the complex perovskite [1]. The structure properties of these materials is extensively studied in solid-state physics and advanced materials science due to the existence of electrical, magnetic high-temperature superconductive properties and others exotic phenomena such as magnetoelectricity, colossal magnetoresistance and half-metallicity [2–5]. These properties offer important perspectives on technological and basic materials science investigations, as well as potential applications in solid oxide fuel cells [6,7]. In recent years, studies about structural properties have shown that several members of the perovskite family adopt a diverse range of structures and, in function of the tolerance factor τ, the perovskites may have a simple cubic structure ($\tau = 1$), with $Fm\bar{3}m$ space group, or can be distorted if $\tau > 1$ or $\tau < 1$, with lower symmetry [8]. Previous studies of structural characterization at room-temperature have shown a wide range of perovskite-type structure in which the Sr_2FeSbO_6, Sr_2SmSbO_6, Sr_2YTaO_6, Sr_2LaSbO_6 and $Sr_2Cd_{1-x}Ca_xWO_6$ doubles perovskites, crystalizes on the monoclinic structure of the $P2_1/n$ space group [9–12]. In the same way, the Sr_2CrSbO_6, Ba_2LaIrO_6 and Ba_2BiSbO_6 adopt the monoclinic structure of the $I2/m$ and R3 space group, respectively [13–15]. Others studies show that the Sr_2CaWO_6 and Sr_2CdWO_6 crystallize in orthorhombic lattices. Similarly, the Sr_2CuWO_6 and Sr_2FeWO_6 crystallize in tetragonal structures and others ones most of the double perovskites crystallizing in lower symmetry lattices [16–21]. On the other hand, the Sr_2EuRuO_6 complex perovskite can be used as precursor oxide for the synthesis of the $RuSr_2EuCu_2O_8$ by the solid-state reaction procedure. This ruthenocuprate material has been investigated because evidences coexistence of magnetic ordering and superconductivity at low temperatures [22]. However, the origin of magnetic behavior in the material family $RuSr_2RECu_2O_8$ (RE = Gd, Dy, Ho, Eu) is still discussed. The aim of this work is to show the synthesis processing, the analysis of the crystalline structure, the superficial morphology and chemical composition of the Sr_2EuRuO_6 complex perovskite. In particular, it is important to note that there are no previous studies about the complete structural characterization of this material. In order to explain these

* Corresponding author. Tel.: +57 1 3165000x13032; fax: +57 1 3165135.
E-mail address: jroar@unal.edu.co (J. Roa-Rojas).

0925-8388/$ – see front matter © 2011 Elsevier B.V. All rights reserved.
doi:10.1016/j.jallcom.2011.12.033

properties, we synthesized the Sr_2EuRuO_6 complex perovskite by the solid-state reaction method and we carry out Rietveld analysis of the experimental Powder X-ray diffraction patterns data (XRDP). In order to characterize the granular feature of compound and obtain the independent elements percentage of the Sr_2EuRuO_6 compound, we performed scanning electron microscopy (SEM) measurements, and we carried out semi-quantitative compositional study by means of energy dispersive X-ray experiments (EDX).

2. Experimental

2.1. Preparation

The ceramic sample of the Sr_2EuRuO_6 material was prepared by the solid-state reaction method from stoichiometric amounts of $SrCO_3$, RuO_2 and Eu_2O_3 (Aldrich 99.99%), to produce samples of 0.35 g. In order to obtain the pure crystallographic phase of the Sr_2EuRuO_6 complex perovskite the initial mixture was ground in an agate mortar and pressed at 2.3×10^{10} Pa to produced cylindrical pellets of 4.9 ± 0.1 mm diameters and 1.2 ± 0.1 mm thickness. For the study of the evolution of crystalline phases, the samples were then annealed in a platinum crucible for 12 h, by four different temperatures; 1123 K, 1173 K, 1223 K, 1303 K and sintered at 1483 K for 24 h.

2.2. Structural characterization

Structural characterization of the Sr_2EuRuO_6 complex perovskite was performed through X-ray diffraction (XRD) measurements in the angular regime $0^\circ \leq 2\theta \leq 90^\circ$ with a step of 0.02°, using a Panalytical Xpert Pro diffractometer *PW1710*, with *CuKα* = 15,406 Å radiation. The Rietveld refinements of the X-ray diffraction patterns were carried out by means of the GSAS code [23]. The results of the Rietveld refinements were compared with characteristic values predicted by the structure prediction diagnostic software (SPuDs), which was created for perovskite-like materials [24].

2.3. Morphological characterization

Morphological studies were performed by means of scanning electron microscopy (SEM) experiments, through the utilization of a FEI Quanta 200. Chemical composition of the samples was analyzed by the energy dispersive X-ray (EDX) technique.

3. Results and discussion

3.1. Structural results

Fig. 1 shows the powder X-ray diffraction patterns for the Sr_2EuRuO_6 complex perovskite after of annealing treatments at 1123 K, 1173 K, 1223 K and 1303 K, respectively, for a same time interval of 12 h. These XRD diffractograms show the systematic evolution of the crystalline phases. In all cases, the prepared sample of Sr_2EuRuO_6 exhibited a crystallized perovskite phase, when is indexed based on the monoclinic $P2_1/n$ lattice. However, one can to observe the existence of a phase corresponding to the Eu_2O_3 (reflections marks with asterisk, Fig. 1), which is close to 18.6% at 1123 K and decreases as a function of the annealing temperature until when reaching a 6.5% for a calcination temperature of 1303 K. This behavior is explained since according to Joint Committee of Powder Diffraction Standard data cards (35-795). The majority of the reflection peaks emerged with a small one (reflections mark with asterisk, Fig. 1) [25]. The formation of the pure crystalline perovskite phase for the Sr_2EuRuO_6 complex perovskite is completed when the sample is annealed at 1483 K for 24 h, as shown in Fig. 2. In this, the continuous curve corresponds to the calculated pattern by means of the GSAS code, and the black crosses represent the experimental data. The verticals short lines on the bottom of picture and the curve show the locations of Bragg peaks and the difference between the experimental pattern and the calculated one respectively. Rietveld refinements of the XRD patterns reveal that at room-temperature the Sr_2EuRuO_6 has a monoclinic perovskite-type structure, which belongs to the $P2_1/n$ (#14) space group, that corresponds to the $(a^+b^-b^-)$ tilt system on the Glazer notation (which is a non-symmorphic space group, and there are two-unit formulas in the unit cell). The presence of (0 1 1), (2 1 1) and (3 −1 0) peaks in the diffractogram of Fig. 2 confirms the existence of the superstructure that characterizes the $A_2M'M''O_6$ complex perovskites [26]. Our results are 99% in agreement with the structure prediction diagnostic software (SPuDs), which predicts $P2_1/n$ (#14) space group as more probable. In this space group the unit cell parameters are related with the primitive unit cell a_p according to; $a = \sqrt{2}a_p$, $b = \sqrt{2}a_p$ and $c = 2a_p$. The formation of the superstructure permits to establish the alternate distribution of the Ru^{5+} (2d: 0.5, 0, 0) and Eu^{3+} (2c: 0.5, 0, 0.5) ions on the six coordinate M sites of the complex perovskite, while the Sr^{2+} is located in the A-site, as shown in Fig. 3.

Another important aspect on the crystal structure of the Sr_2EuRuO_6 complex perovskite ($P2_1/n$ (#14) space group) is its distortion from the ideal cubic perovskite structure. This distortion is easily explained if we take into account that the Sr_2EuRuO_6 have the generic formula of the superstructure $A_2M'M''O_6$ and since by this type of materials if the tolerance factor $\tau < 1$, then the structure

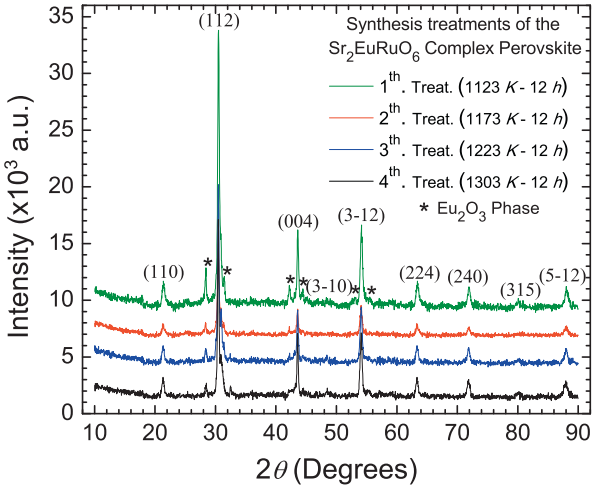

Fig. 1. X-ray diffraction pattern for the Sr_2EuRuO_6 complex perovskite after of calcined treatments at 1123 K, 1173 K, 1223 K and 1303 K, respectively, for a same time interval of time of 12 h.

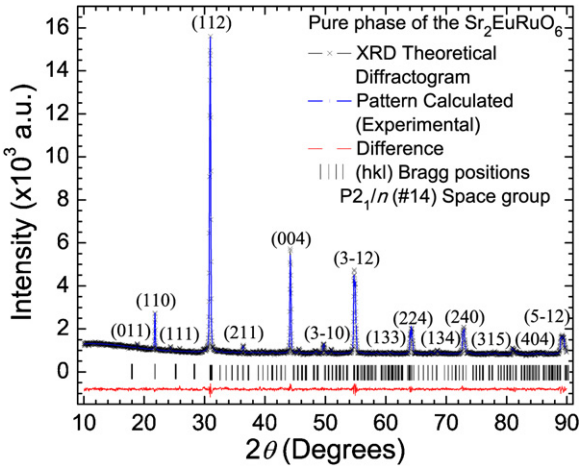

Fig. 2. X-ray diffraction pattern of the pure crystalline perovskite phase by the Sr_2EuRuO_6 complex perovskite at 1483 K. The XRDP corresponds to the monoclinic $P2_1/n$ (#14) space group.

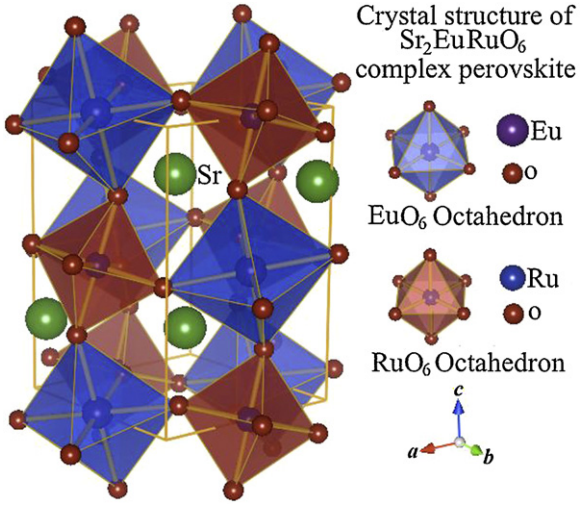

Fig. 3. Crystal structure of the Sr_2EuRuO_6 complex perovskite belong to the $P2_1/n$ (#14) space group. The cube in continuous line indicates the primitive unit cell a_p.

have lower symmetry. The tolerance factor τ is calculated by the ratio

$$\tau = \frac{r_A + r_o}{\sqrt{2}((r_{M'} + r_{M''}/2) + r_o)}, \quad (1)$$

where r_A, $r_{M'}$, $r_{M''}$ and r_o are the ionic radii of A, M′, M″ and O ions, respectively. In agreement with the prediction of SPuDs, and ratio (1) the tolerance factor value for the Sr_2EuRuO_6 is close to $\tau = 0.9073(6)$. Additionally, in the crystal structure of the Sr_2EuRuO_6 the $EuO_{6/2}$ and $RuO_{6/2}$ octahedral maintain the union between their corners, while support the tilting of the $EuO_{6/2}$ and $RuO_{6/2}$ octahedral. Therefore, the Sr_2EuRuO_6 complex perovskite undergo a decrease in its symmetry. Afterward, the Ru^{5+} and Eu^{3+} cations are located on two crystallographic independent octahedral sites called 2*d* and 2*c* [27]. In order to clarify this behavior, Fig. 4a shows the tilting around the plane $[h\,k\,l]_P = [1\,0\,0]_P$. The average tilt angle of the $EuO_{6/2}$ and $RuO_{6/2}$ octahedral is calculated by the ratio

$$\sigma = \frac{180 - \varphi}{2}, \quad (2)$$

where φ is the average Eu—*O*—*Ru* inter-atomic bond angle, in agreement with ratio (2) and the average Eu—*O*—*Ru* inter-atomic bond angle, shown in Fig. 4a, we obtain that the average tilt angle for the $EuO_{6/2}$ and $RuO_{6/2}$ octahedral are close to 18.28° and 22.37°, respectively. These results are 99% in agreement with the SPuDs,

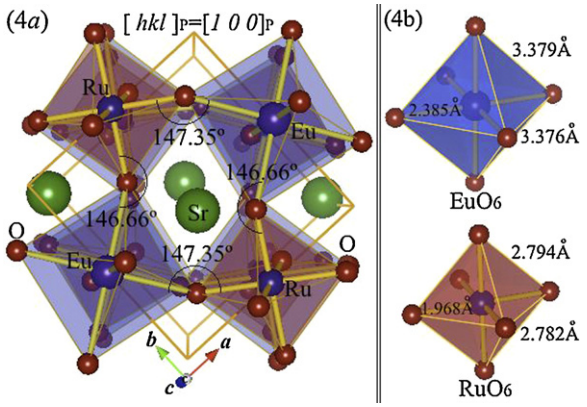

Fig. 4. Tilting of the $EuO_{6/2}$ and $RuO_{6/2}$ octahedral around the plane $[h\,k\,l]_P = [0\,0\,1]_P$ (a), and main inter-atomic distances Eu—O and Ru—O on the $EuO_{6/2}$ and $RuO_{6/2}$ octahedral (b).

which predicts 18.31° and 22.41°, respectively. This tilting of the octahedral occurs because the $EuO_{6/2}$ and $RuO_{6/2}$ octahedral is constrained to tilt so as to optimize the *Sr*—*O* inter-atomic bond length, since the Ru^{5+} cation is smaller than the Eu^{3+} cation. In Fig. 4b, some-inter atomic bond lengths Eu—*O* and *Ru*—*O* in the $EuO_{6/2}$ and $RuO_{6/2}$ octahedral are shown. One can see that the axial bond lengths are lightly longer than equatorial bond lengths, this lead to tilting of the $EuO_{6/2}$ and $RuO_{6/2}$ octahedral [28]. The main inter-atomic bond lengths, main inter-atomic bond angles and others important structural parameters obtained from Rietveld refinements of the X-ray diffraction patterns by the Sr_2EuRuO_6 complex perovskite, are shown in Table 1.

3.2. Morphological results

The agglomerates and the particle size are important issues in the study of the crystal structure and morphology of the Sr_2EuRuO_6 complex perovskite, since the particle size and the uniformity of the size distribution sets the microstructure affect the properties of the compound. In addition, the microstructure of sintered of the ceramic sample strongly influence the mechanical, thermal, electrical, and magnetic properties, and the chemical corrosion resistance [29]. Previous studies of materials of the perovskite class has shown that some properties such as; ferroelectricity, electrical permittivity and structure are strongly related to the particle size [30]. Particularity, the particle size effect on dielectric properties has been intensively studied for $BaTiO_3$ perovskite [31]. In order to obtain the pure perovskite phase and a dense sample of the Sr_2EuRuO_6 ceramic material with uniform particle size after the sintering process, we control the particle size, morphology of agglomerates and distribution of the size of aggregates of grains, using precursor powders with an appropriate distribution of particle size. Likewise, we performed a prolonged milling process so as to produce a homogenization of the particle size on the compound. Because the particle size increases as the annealing temperature increases, and taking into account that the average particle size in the sample increases slightly with sintering time, the heating at constant rate was performed in order to set the sintering temperature. In this way the particle sizes obtained by the different annealing temperatures are attributed to the high temperature process, which improves the reactivity of the precursor powders as the compound reaches the pure perovskite phase [32]. In order to analyze the surface morphology and calculate the particle size of the Sr_2EuRuO_6 complex perovskite, we use the X-ray diffraction pattern data shown in Figs. 1 and 2. The particle size was calculated by using the Scherrer equation, which is based on widening of maximum intensity weak of X-ray diffraction pattern due to particle size exclusively [33], and defined by the ratio

$$D = \frac{K\lambda}{\beta(\theta)\cos\theta}, \quad (3)$$

where D is the average particle size, $K = 0.89$ nm is the Scherrer constant, λ is the X-ray wavelength radiation, that in our case corresponds to $\lambda = 0.15406$ nm and β is the half-peak width of the diffraction profile. Fig. 5, shows the average particle size calculated using the Scherrer equation, and based on the half-width of the Sr_2EuRuO_6 (1 1 2) peaks, by the five X-ray diffraction patterns shown in Figs. 1 and 2. The particle size of the Sr_2EuRuO_6 complex perovskite annealed for a time of 12 h, at the temperatures of 1123 K, 1173 K, 1223 K and 1303 K are close to 12.3 nm, 14.9 nm, 16.8 nm and 22.9 nm, respectively, while for the sintered temperature of 1483 K corresponds to 34.2 nm. These results are in agreement with the scanning electron microscopy (SEM) measurements, realized by the Sr_2EuRuO_6 material, and shown in Fig. 6, at 1123 K, and in Fig. 7, at 1483 K. The SEM micrograph at 1123 K shows that the particles of the sample make up small

Table 1
Structural parameters of the Sr_2EuRuO_6 complex perovskite obtained by Rietveld refinements of the X-ray diffraction patterns.

Space group: $P2_1/n$ (#14)						
Unit cell parameters obtained from Rietveld refinements of the X-Ray diffraction (XRD) patterns						
a = 5.7996(5) Å	b = 5.8960(7) Å	c = 8.3234(6) Å	β = 90.234(7)°	V = 284.61(4) Å^3	τ = 0.9073(6)	
Powder data statistics from Rietveld refinements						
χ^2 = 1.145	R_F = 4.6%	R_{wp} = 3.47%	R_P = 3.07%	R_e = 3.21%		
Atomic positions obtained from XRDP analysis						
Atom	Sr	Eu	Ru	O (1)	O (2)	O (3)
Site	4*e*	2*c*	2*d*	4*e*	4*e*	4*e*
x (Å)	0.53392(3)	0.00000(0)	0.50000(0)	0.23145(1)	0.32878(2)	0.40931(8)
y (Å)	0.57349(2)	0.50000(0)	0.00000(0)	0.18431(3)	0.73197(5)	0.97986(6)
z (Å)	0.25132(6)	0.00000(0)	0.00000(0)	0.94750(4)	0.93274(3)	0.21878(4)
Main inter-atomic distances and valences						
Cation	Anion	Multiplicity	Distance (Å)	Valence	Main bond angles (°).	
Eu (2c)	O (4e)	×2	2.39578(1)	0.51872(3)	Eu(2c)-O(4e)-Ru(2d)	147.35(4)
Eu (2c)	O (4e)	×2	2.39673(4)	0.50031(1)	Eu(2c)-O(4e)-Ru(2d)	146.66(2)
Eu (2c)	O (4e)	×2	2.38501(1)	0.51001(1)	Eu(2c)-O(4e)-Ru(2d)	147.38(3)
Ru (2d)	O (4e)	×2	1.95056(7)	0.83210(5)	O(1)-Eu-O(2)	89.962(1)
Ru (2d)	O (4e)	×2	1.96643(5)	0.82982(1)	O(2)-Eu-O(3)	90.291(3)
Ru (2d)	O (4e)	×2	1.96811(1)	0.83678(2)	O(3)-Eu-O(3)	88.798(5)

agglomerates which vary size and morphology, while the SEM micrograph at 1483 K shows that the agglomerates are more distributed uniformly on the simple, with a random distribution from amongst ≈1 to 3 μm size. This behavior of the agglomerates is due to the assembly of small grains in the sample. Fig. 8 shows the spectra of energy dispersive X-ray (EDX) for the independent elements of the Sr_2EuRuO_6 compound. This figure reveals that the small grains in the sample consist of Sr, Eu, Ru and *O* in the atomic concentrations shown in Table 2. The differences between theoretical and experimental weight percentage values of the individual elements obtained from stoichiometric calculations and semi-quantitative EDX experiments occur because the oxygen has a little weight for scattering of X-ray radiation. Experimental weight percentages are in agreement with the theoretical expected values, as shown in Table 2. Fig. 9 shows the percentage of pure perovskite phase of the Sr_2EuRuO_6 as a function of the annealing temperature for each one of the particle size obtained. One can see that the monoclinic $P2_1/n$ phase of the Sr_2EuRuO_6 increases as the particle size increases, since for all X-ray diffraction patterns shown in Figs. 1 and 2, the particle size increases as the annealing temperature increases. When the particle size corresponds to 12.3 nm, the X-ray diffractions patterns of the Sr_2EuRuO_6 could be indexed by a structure belong to monoclinic phase of the I2/*m* and $P2_1/n$ lattice. Nevertheless, the Rietveld refinements performed using the symmetry of the monoclinic I2/*m* (#12) space group no matching adequately with the experimental patterns and the reliability factor presents a high error in the relation percentage. As the particle size increases from 14.9 nm toward a value of 34.2 nm at 1483 K, the (0 1 1), (1 1 0) and (1 1 1) peak splitting appear in the diffractogram at 19.2°, 21,8° and 24,6°, respectively (see Fig. 2), which suggest that the unit cell is monoclinic. Furthermore, these reflections in the XRD pattern indicate the presence of cationic ordering and super-structure reflections. The simultaneous presence of in-phase and out-of-phase tilting, involves a new orientation of the lattice to lowering of the crystal symmetry toward $P2_1/n$ space

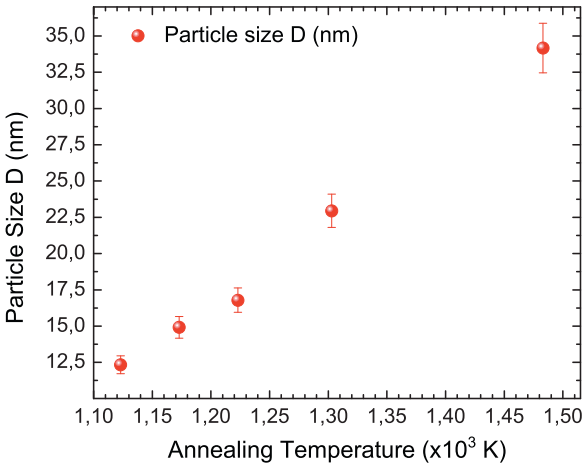

Fig. 5. Average particle size calculated using the Scherrer equation, and based on the half-width of the Sr_2EuRuO_6 (1 1 2) peaks.

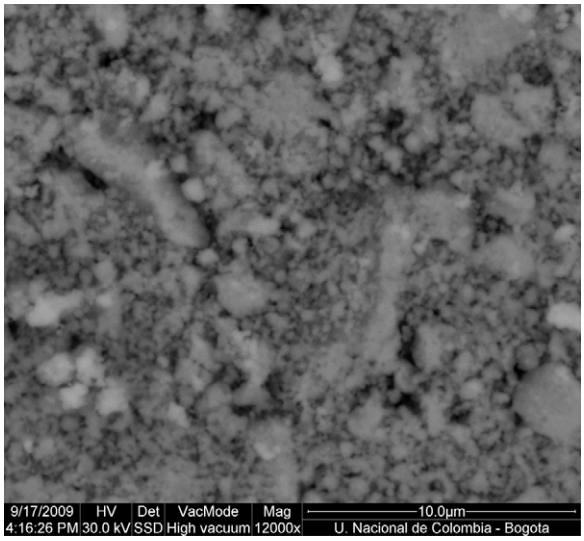

Fig. 6. Scanning electron microscopy (SEM) measurements, realized by the Sr_2EuRuO_6 material at 1123 K, small agglomerates which vary size and morphology are shown.

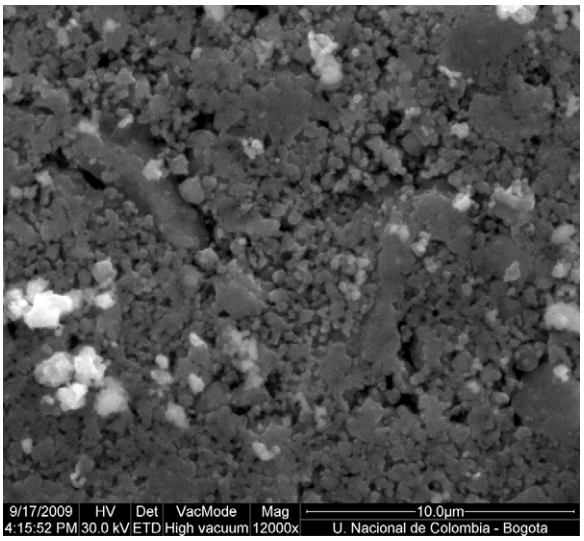

Fig. 7. Scanning electron microscopy (SEM) measurements, realized for the Sr_2EuRuO_6 material at 1483 K, the particles are distributed uniformly on the simple with a random distribution of agglomerates.

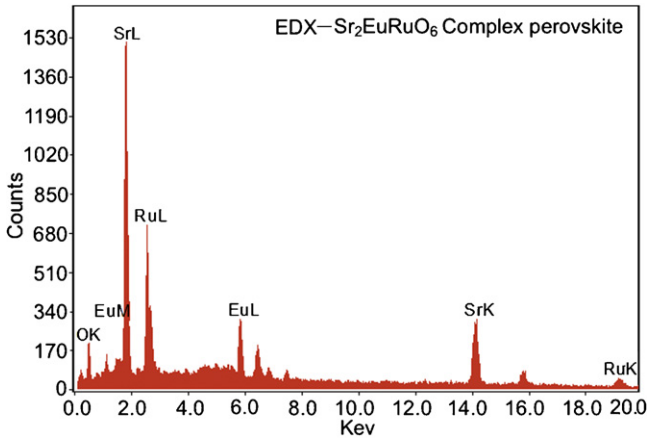

Fig. 8. Energy dispersive X-ray (EDX) spectra measurements of the individual's elements of the Sr_2EuRuO_6 compound.

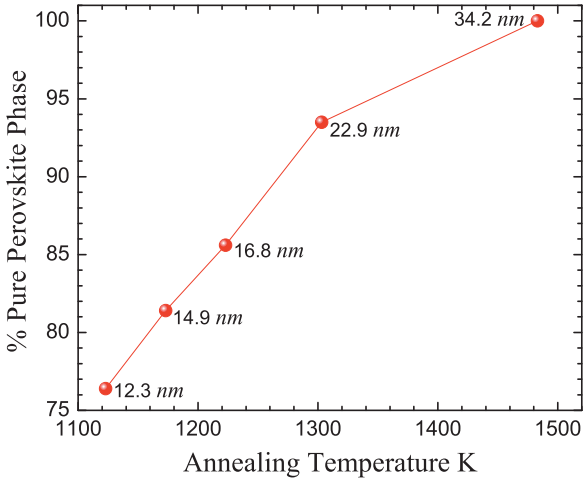

Fig. 9. Percentage of pure perovskite phase of the Sr_2EuRuO_6 as a function of the annealing temperature for each one of the particle size obtained.

Table 2
Stoichiometric and weight percentage of the Sr_2EuRuO_6.

Atom	Sr	Eu	Ru	O
Stoichiometric	2	1	1	6
(%) Weight (Expe.)	33.86	32.12	19.93	14.09
(%) Weight (Theo.)	32.77	30.38	18.90	17.95
(%) Difference	3.33	5.73	5.45	21.50

group. Another important fact is that the crystal structure of the Sr_2EuRuO_6 suffers a decrease of the lattice parameters and consequently the unit cell volume decreases as the particle size increases; this could be due to decreasing of the ratio of surface to volume with increasing the particle size. This result suggests that for a particle size close to 34 nm the crystal structure of the Sr_2EuRuO_6 suffers grain size-induced polarization rotation, which produces a phase transition toward monoclinic phase $P2_1/n$ (#14). On the other hand, the increase of the annealing temperature or the sintering time increases the grain size of material, while changing the grain morphology from the common plate-like form observed in ceramics, toward a spherical-like form, as shown in Fig. 7. These phenomena generally produce a decrease in surface tension and this leads to a decrease of lattice parameters or a transformation of crystallographic structure toward a low symmetric [34], which in our case corresponds to the monoclinic $P2_1/n$ (#14) space group. Because the grain size is dependent on the nucleation rate and the growth rate, respectively, then the particle size obtaining for the Sr_2EuRuO_6 by the solid-state reaction procedure is attributed to the decomposition reaction toward oxides, which may be responsible for the refinement of the particle size [35]. The state solid reaction process destroys the origin morphologies of the precursor powders, and then fine particles with similar size distributions may be obtained. These fine particles are able to agglomerate once and again and this lead to the similar size distributions of the agglomerates shown in Fig. 7. On the other hand, the particle size obtained for the Sr_2EuRuO_6 morphology suggests that the influence of the sliding processes decreases as increase grain sizes of the compound [36]. In addition, ceramics samples with small particle sizes suffers a large amount of grain boundaries, which are responsible of sliding processes, because the grain boundaries as amorphous areas surrounding crystalline cores promotes the sliding processes [37].

Another one important fact in the synthesis process of the Sr_2EuRuO_6 complex perovskite is the activation energy E_a, which is defined as the energy barrier that must be surmounted during transformation of reactive powders into final ceramic sample during the rate-limiting step [38]. However, in others studies have been suggested that the activation energy E_a is the average excess energy that a reactant molecule must possess to react [39]. The analysis of the activation energy E_a and reaction rate allows to determinate the reaction mechanisms in solid phases, and if there are changes in the reaction mechanisms then is possible understand the material properties. Previous studies performed by Celis et al. [40], have shown that the activation energies E_a for the intermediates in the thermal decomposition is particularly sensitive to the overlap in thermal decomposition traces. This phenomenon leads to a large variations of the activation energy E_a with the extent of conversion and can be influenced by the altering the conditions on the measurements that are performed in the isothermal and non-isothermal experiments [41]. The activation energy E_a can be calculated by means of the Arrhenius equation given by

$$\frac{d\ln k}{dT} = \frac{E_a}{RT^2}, \tag{4}$$

where k corresponds to the specific reaction rate constant, E_a is the activation energy, $R = 8.314$ J/mol is the universal gas constant and T

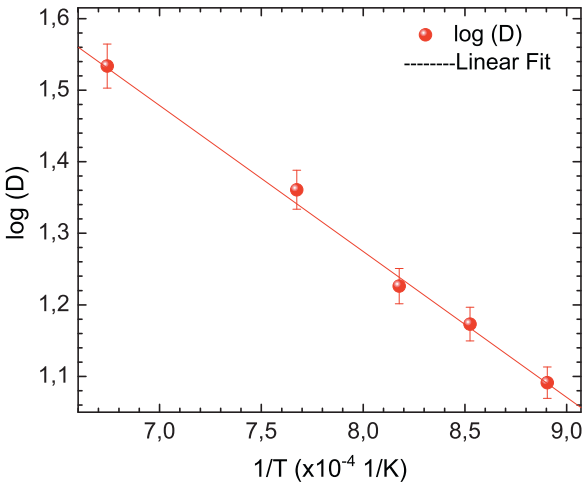

Fig. 10. Relationship between log D and $1/T$ know as Arrhenius plot.

is the absolute temperature [42]. Previous studies have shown that the k value in eq. (4) is related with the particle size [43] through the ratio

$$\log\ D = -\frac{E_a}{2.303RT} + A, \tag{5}$$

where D is the particle size and A is a constant value. Fig. 10 shows the relationship between log D and $1/T$, whose intercept corresponds to the constant A and the slope is equal to $-E_a/(2.303R)$, take T = 298 K (room-temperature). From the results obtained, we found that the activation energy E_a for the Sr_2EuRuO_6 complex perovskite is close to E_a = 39.6 kJ/mol. This value of the activation energy E_a suggest that during the sintering process of the Sr_2EuRuO_6 complex perovskite oxygen species are delivering that should in fact lower the activation energy E_a of the compound [44]. Also the activation energy E_a suggests that the ion mobilities on the Eu_2O_3 and RuO_2 phases are lower than in alkaline earth metal Sr because the lack of framework modifiers of alkaline earth metal Sr ions in the Eu_2O_3 and RuO_2 phases. Besides this, during the sintering process of the Eu_2O_3 oxide, the O_2 partial pressure in the atmosphere is able to take a value that maintains the Eu atoms in the oxidation state +3. Also, the observed low value of the activation energy E_a in the Sr_2EuRuO_6 sample may be due to the presence of charges carriers inside the grains [45]. Because the particle size found for the Sr_2EuRuO_6 are in the range of nanometers and taking into account that the sintering temperature by the Sr_2EuRuO_6 was fixed in the range near to 1483 K. It can be conclude that the densification rate of particle size in the Sr_2EuRuO_6 is high. This can be suggested since the activation energy E_a is a composite function made up by the contributions of several parameters that involve the deviation from equilibrium and the thermal gradient [46], and increasing temperatures resulted in significant reduction in the magnitude of the activation energy E_a. Because the Sr_2EuRuO_6 sample was heated at constant rate until reach up to the isothermal sintering temperature and since the activation energy E_a for Sr_2EuRuO_6 is close to E_a = 39.6 kJ/mol, it is can corroborate that the Sr_2EuRuO_6 sample has a high densities as the particle size and a uniformity of the size distribution is controlled on the compound. The low value of the activation energy E_a suggests that the Sr_2EuRuO_6 sample undergoes a rapid and complete nucleation of the precursors powders at all edges of the platelike crystallites, where the kinetics of decomposition was strongly influenced by the morphology of the reactant powders.

4. Conclusions

We have carried out an experimental study of the synthesis process, the crystal structure as well as the surface morphology of the Sr_2EuRuO_6 complex perovskite. Rietveld analyses show that this compound crystallizes in a monoclinic distorted perovskite-type structure, which belongs to the monoclinic $P2_1/n$ (#14) space group. The structure presents an alternating distribution of the Ru^{5+} and Eu^{3+} ions, on the six coordinate M sites, while the Sr^{2+} is located in the A-site. Morphological analysis of material, performed by SEM, allowed to establish the granular feature of compound with agglomerates from amongst ≈1 to 3 μm size, and by means of the Scherrer formula the particle size was calculated to be D = 34.2 nm. The monoclinic $P2_1/n$ phase of the Sr_2EuRuO_6 increases while the lattice parameters and the unit cell volume decreases as the particle size increases due to decreasing of the ratio of surface to volume with increasing particle size. Our result suggests that the crystal structure of the Sr_2EuRuO_6 suffers grain size-induced polarization rotation, which produces a phase transition toward monoclinic phase $P2_1/n$ (#14). The increase of the annealing temperature or the sintering time increases the grain size of material, while changing the grain morphology from plate-like toward a spherical-like form. This produces a decrease in surface tension and this leads to a decreases of lattice parameters or a transformation of crystalline structure toward the low symmetric monoclinic $P2_1/n$ (#14). The particle size and the morphology of the Sr_2EuRuO_6 suggest that the influence of the sliding processes decreases with the increasing of the grain sizes of the compound. The activation energy E_a calculated by means of the Arrhenius plot for the Sr_2EuRuO_6 complex perovskite is close to E_a = 39.6 kJ/mol, suggesting that during the sintering process of the Sr_2EuRuO_6, are delivered oxygen species that should lower the activation energy E_a of the compound. The low value of E_a in the Sr_2EuRuO_6 may be due to the presence of charges carriers inside the grains. The Sr_2EuRuO_6 sample has high densities when the particle size and the uniformity of the size distribution are controlled on the compound, and the densification rate of particle size in the Sr_2EuRuO_6 is high. The value of the activation energy E_a suggests that the Sr_2EuRuO_6 undergoes a rapid and complete nucleation of the precursor powders and the kinetics of decomposition is strongly influenced by the morphology of the reactant powders.

Acknowledgements

This work was partially supported by the Colombian agencies Division of Investigations of the Universidad Nacional de Colombia-Bogotá D.C. (DIB-Bogotá) and CENM on the "El Patrimonio Autónomo Fondo Nacional de Financiamiento para la Ciencia, la Tecnología y la Innovación Francisco José de Caldas" Contract RC-No. 275-2011.

References

[1] Y. Doi, Y. Hinatsu, J. Phys. Condens. Matter 11 (1999) 4813–4820.
[2] S. Jin, T.H. Teifel, M. McCormack, R.A. Fastacht, R. Ramesh, L.H. Chen, Science 254 (1994) 413.
[3] C. Zhong, J. Fang, Q. Jiang, J. Phys. Condens. Matter 16 (2005) 9059.
[4] K.I. Kobayashi, T. Kimura, H. Saeada, K. Tekura, Y. Tokura, Nature 395 (1988) 677.
[5] B.G. Landa, C. Ritter, M.R. Ibarra, J. Blasco, P.A. Algarabel, R. Mahendiran, J. Garcia, Solid State Commun. 110 (1999) 435.
[6] T. Xia, Q. Li, J. Meng, X. Cao, Mater. Chem. Phys. 111 (2008) 335.
[7] Y.H. Huang, G. Liang, M. Craft, M. Lehtimaki, M. Karppinen, J.B. Goodenough, Chem. Mater. 21 (2009) 2319.
[8] W.T. Fu, D. Visser, K.S. Knight, D.J.W. Ijdo, J. Solid State Chem. 177 (2004) 1667–1671.
[9] A. Faik, j.M. Igartua, E. Iturvbe-Zabalo, G.J. Cuello, J. Mol. Struct. 963 (2010) 145–152.
[10] A. Faik, J.M. Igartua, J.L. Pizarro, J. Mol. Struct. 920 (2009) 196–201.

[11] A. Faik, E. Iturvbe-Zabalo, I. Urcalay, j.M. Igartua, J. Solid State Chem. 182 (2009) 2656–2663.
[12] Q. Zhou, B.J. Kennedy, M. Avdeev, J. Solid State Chem. 183 (2010) 1741–1746.
[13] A. Faik, j.M. Igartua, M. Gateshki, G.J. Cuello, J. Solid State Chem. 182 (2009) 1717–1725.
[14] M. Gateshki, J.M. Igartua, Mater. Res. Bull. 38 (2003) 1893–1900.
[15] M.W. Lufaso, R.B. Macquarta, Y. Leeb, T. Vogta, H.C. Loye, J. Solid State Chem. 179 (2006) 917–922.
[16] Z.M. Fu, Sci. Chin. Ser. A 34 (1991) 455.
[17] Z.M. Fu, W.X. Li, Sci. Chin. Ser. A 38 (1995) 974.
[18] D. Reinen, H. Weitzel, Z. Anorg. Allg. Chem. 424 (1976) 31.
[19] A.K. Azad, S.A. Ivanov, S.G. Eriksson, J. Eriksen, H. Rundolof, R. Matheieu, P. Svedlindh, Mater. Res. Bull. 36 (2001) 2215.
[20] G. Blasse, J. Inorg. Nucl. Chem. 27 (1965) 993.
[21] M. Gateshki, J.M. Igartua, J. Phys. Condens. Matter 16 (2004) 6639.
[22] L.T. Yanga, J.K. Lianga, Q.L. Liua, C.Q. Jina, X.M. Fenga, G.B. Songa, J. Luoa, F.S. Liua, G.H. Rao, J. Solid State Chem. 177 (2004) 1072.
[23] A.C. Larson, R.B. Von Dreele, General Structure Analysis System (GSAS) Los Alamos National Laboratory Report, Laur, 2000, p. 86.
[24] M.W. Lufaso, P.M. Woodward, Acta Crystallogr. B 57 (2001) 725.
[25] W.F. Yao, X.H. Xuc, H. Wang, J.T. Zhoua, X.N. Yang, Zhang, S.X. Shang, B.B. Huang, Appl. Catal. B: Environ. 52 (2004) 109–116.
[26] O. Ortiz Diaz, J. Roa-Rojas, D.A. Landínez Téllez, J. Albino Aguiar, Mod. Phys. Lett. B 18 (2004) 1035.
[27] R. Sáez-Puche, E. Climent-Pascual, R. Ruiz-Bustos, M.A. Alario-Franco, M.T. Fernández-Díaz, Prog. Solid State Chem. 35 (2007) 211–219.
[28] R. Shaheen, J. Bashir, Solid State Sci. 12 (2010) 1496.
[29] J.J. Zuckerman, D. Jim, Atwood, Inorganic Reactions and Methods, Formation of Ceramics, vol. 18, Wiley-VCH, Inc., 1999, p. 3.
[30] K. Kinoshita, A. Yamaji, J. Appl. Phys. 47 (1976) 371.
[31] Z. Zhao, V. Buscaglia, M. Viviani, M.T. Buscaglia, L. Mitoseriu, A. Testino, et al., Phys. Rev. B 70, 024107 (2004) 1–8.
[32] F. Rubio, P. Ochoa, J.F. Fernandez, J. Eur. Ceram. Soc. 27 (2007) 4125–4129.
[33] B.D. Cullity, Elements of X-ray Diffraction, 2nd edition, Addison Wesley Publishing Company, Inc., Reading, MA, 1978.
[34] B.D. Begg, K.S. Finnie, E.R. Vance, J. Am. Ceram. Soc. 79 (1996) 2666–2672.
[35] Z. Yuhua, L. Jing-Feng, J Am. Ceram. Soc. 89 (2006) 3669–3675.
[36] W. Schatt, V. Festphasensintern, I. Verallgemeinerungsfähigkeit, Metallkde 80 (11) (1989) 809–816.
[37] Y. Dror, R.D. Levi, S. Baltianski, Y. Tsur, J. Electrochem. Soc. 153 (7) (2006) F137–F143.
[38] C.H. Bamford, C.F.H. Tipper, Comprehensive Chemical Kinetics, vol. 22, Elsevier Scientific Publishing Company, 1980.
[39] J.P. Redfern, R.C. MacKenzie (Eds.), Differential Thermal Analysis, vol. 1, Academic Press, New York, 1970, p. 123.
[40] K. Celis, I. Van Driessche, R. Mouton, G. Vanhoyland, S. Hoste, Euro Ceram. VII (2002) 1–3.
[41] K. Celis, I. Van Driessche, R. Mouton, G. Vanhoyland, S. Hoste, Meas. Sci. Rev. 1 (2001) (Number 1).
[42] Y.S. Changa, Y.H. Changa, I.G. Chena, G.J. Chenb, Y.L. Chai, J. Crystal Growth 243 (2002) 319–326.
[43] M. Jarcho, C.H. Bolen, R.H. Doremus, J. Mater. Sci. 11 (1976) 2027.
[44] D. Fino, N. Russo, G. Saracco, V. Specchia, J. Catal. 217 (2003) 367–375.
[45] N. Hirose, A.R. West, J. Am. Ceram. Soc. 79 (1996) 1633.
[46] G. Bertrand, M. Lallemant, G. Watelle, J. Therm. Anal. 13 (1978) 525.